Next Generation Cavitation Monitoring Devices

Yang Hou

China Academic of Electronics and Information Technology, Beijing 100000, China.

Abstract: This study aims to design and construct a passive cavitation detector(PCD), which has high sensitive to low frequency components of periodic shock waves. This device will feature a geometrically focused, curved active element surface, A finite element model in PZflex was created to simulate the detecting process of the focused shock wave passive cavitation detector (PZflex). And the performance is evaluated against the novel shock wave passive cavitation detector (swPCD), which was designed and constructed by the cavitation laboratory (Cavlab), medical and industrial ultrasonic (MIU).

Keywords: Passive Cavitation Detector; PZflex; swPCD

1. Theoretical model of spectral analysis on periodic shock waves

As introduced in the previous section, it is found that periodical shock waves generated from acoustic cavitation are characteristic signals that can be used to detect and measure cavitation. Therefore, a theoretical generic model that evaluates the effects of periodical shock waves on the signal spectrum of cavitation is developed, which considers and describes five common periodical shock waves (referred to as PSW in the following symbols), including: (1) *x*PSW (T), illustrates an ideal example of the periodical emission of *x*PSW (t); (2) the peak-positive pressure amplitude, PPPASW , is constant for each component shocwave, and (3) *T*PSW . A shock wave function of *x* PSW (t) can be described as following *x*PSW(*t*)=*cT*(*t*) x *wD*(*t*)**s*(*t*),(1)where *cT*(*t*) is an impulse train, which is multiplied and convolved with *wD*(*t*), representing a rectangular window function in which *D* connotes the period of the shockwave train, and *s*(*t*) is a function of the shockwave shown in Figure 1(b). Furthermore, *cT*(*t*) can be represented as

$$c_T(t) = \sum_{k=-\infty}^{\infty} 6\left(t - \frac{k}{T_{PSW}}\right), (k \in N),$$

where 6 is the Dirac delta function and *wD*(*t*) = $\prod$(*t*/*D*).

Besides, *X*PSW (*f*), the Fourier transform of equation (1) is accordingly expressed as following:

$$X\text{PSW}(f) = CT(f) * WD(f) \times S(f), \qquad (2)$$

Where $CT(f) = \frac{1}{TPSW \sum_{k=-\infty}^{\infty} 6\ (t - 2\pi fPSW\ k)}$,(k∈N), and *f*PSW=1/*T*PSW, *S*(*f*) is the spectrum of an individual shock wave, and *W*D(*f*) = *D* sinc (*fD*). Figure 1(a) illustrates the spectrum of Figure 1(a), which indicates that periodical shock waves can display as a series of peaks at *nf*PSW, and *CT*(*f*), i.e. the Fourier transform of *c*T (*t*) is itself an impulse train. For each spectral peak, the width is established by *WD*(*f*), which is the FT Fourier transform of *wD*(*t*). The strength of these spectral peaks reduce at a similar rate to the spectral content of the shock wave, *S*(*f*), as shown in Figure 1(b). Besides, due the shorter timeframe in the window function, the spectral peaks for the represented three shock waves are wider than those for five, as shown in Figure 1(b).

Consequently, for a cavitation cloud induced by the external ultrasound field at a fundamental frequency *f*0 , in a regime where strong collapses of the cloud occur, leading to the emission of shock waves at the half-harmonic, i.e., *f*PSW = *f*0 / 2, the periodical shock waves can be considered to make a contribution to all spectral features at

$nf0$ / 2, including $nf0$.

It is reported that the increase in the pressure strength of the external acoustic field will generate collapses of cavitation cloud occurring at higher-order sub-multiples, $nf0 = m$, for $m > 2$, and for these regimes, periodical shock waves may be considered to make a contribution to all features at $nf0 = m$.

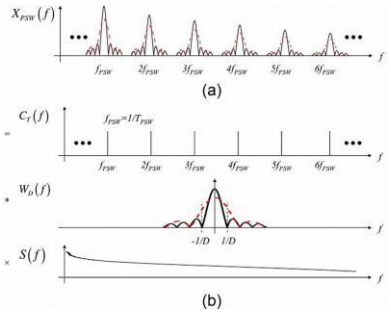

Figure 1 Illustration of the theoretical model of spectral analysis for periodic shock waves, in the frequency domain, where red dash represents three shock waves, and solid black represents five shock waves.

2. Method and material

2.1 swPCD Experimental model

2.1.1 Construction of swPCD

This topic selects swPCD with effective size of 15mm as the reference model, and its simulation model is shown in Figure 3.1 in PZflex.

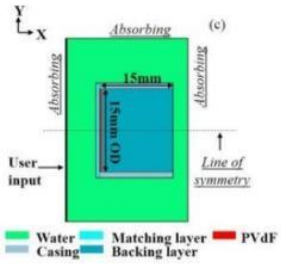

Fig.3.1 construction of swPCD [39]

The main components of the swPCD simulation model are the backing layer, matching layer and the PVdf film. By adjusting the parameters of the backing layer and the matching layer, the detector obtains the best sensitivity for shock wave detection.

2.2 fswPCD Experimental model

2.2.1 construction of fswPCD

In order to compare performance with the original swPCD model, a focused shock wave passive cavitation detector (fswPCD) model was created in PZflex. A schematic diagram of its construction is shown in Fig 3.4

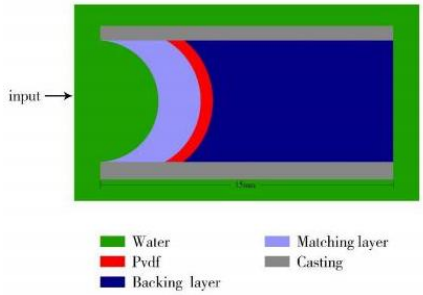

Fig 3.4 construction of fswPCD

Compared to the swPCD model, the fswPCD model uses the same material and thickness of matching layer and backing layer, but makes the front surface and interfaces between 3 materials become curved. The purpose of this structural change is to make the detector obtain higher sensitivity when detecting shock waves, because as mentioned in the 2.4 section, the shock wave generated by bubble collapse is generally arc-shaped, When the shock wave is in contact with the detector surface, the arc surface can better meet the geometric characteristics of the shock wave.

3.1 Detection of a plane wave by swPCD

Fig 4.1 (a) shows the results in the time domain obtained when swPCD detects a plane wave. The distance between source and swPCD is set as 2mm. Under this condition, the peak-normalised output is 37.78mV, this value appears when the simulation model runs at 5.741 μs. It can be seen from the experimental results that when using swPCD to detect a plane wave, the rise-time (RT) is 0.417μs (from 5.324 μs to 5.741 μs) and the full-width-half-maximum (FWHM) is 0.314μs (from 5.597 μs to 5.911 μs). Fig 4.1 (b) depicts the spectra for this detection in frequency domain, its frequency domain characteristics indicate the sensitivity of the detector to this type of shock wave. As can be seen in Fig 4. 1(b), for frequency < 10MHz, the magnitude value concussive decline from 0dB to around - 150dB. For the higher frequency components, there is no significant decline in detector sensitivity.

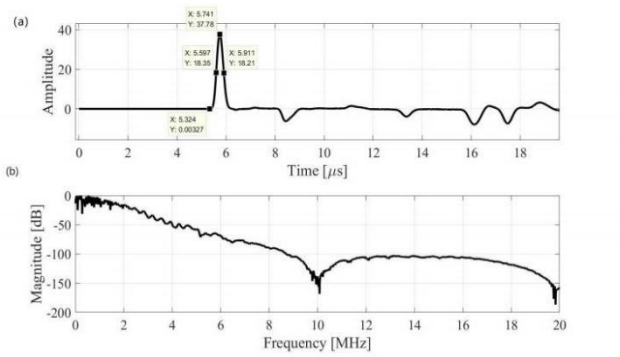

Fig 4.1 (a) result of detecting a plane wave by swPCD in time domain. (b) result of detecting a plane wave by swPCD in frequency domain.

3.2 Detection of a plane wave by fswPCD

As mentioned in section 3.3, in order to explore the effect of different detection surface curvature on the performance of fswPCD, three different radians were used for testing in this experiment. Fig 4.2 presents the result of detecting a plane wave by fswPCD in time domain, when the radius of top surface of cylinder r =14mm, the longitudinal length of fswPCD H = 16.62mm. The distance between source and fswPCD keeps the same with measurement in 4.1 (2mm).

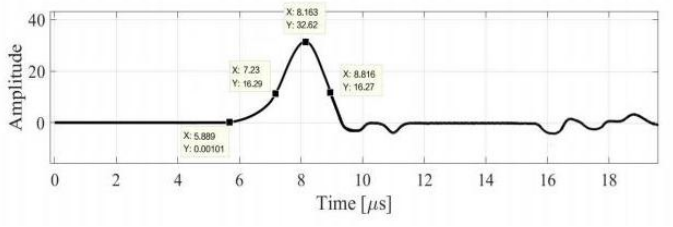

Fig 4.2 the result of detecting a plane wave by fswPCD in time domain , r=14mm, H=16.22mm

Under this condition, the peak-normalised output is 32.62mV, reduced by 13.6% (5.16mV) compared to the results of 4.1, this value appears when the simulation model runs at 8.163 μs. The rise-time (RT) is 2.274 μs (from 5.889μs to 8.163μs) and the full-width-half-maximum (FWHM) is 1.586 μs (from 7.23 μs to 8.816 μs). The RT and FWMH increased by 1.857 μs and 1.272 μs respectively.

Fig 4.3 shows the fswPCD result in time domain, when the radius of top surface of cylinder r = 12mm, the longitudinal length of fswPCD H = 17.31mm.

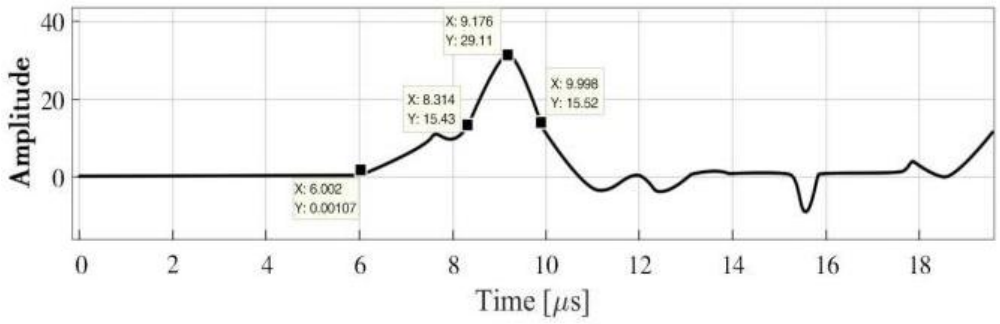

Fig 4.3 the result of detecting a plane wave by fswPCD in time domain , r=12mm, H=17.31mm

Under this condition, the peak-normalised output is 29.11mV, reduced by 22.9% (8.67mV) compared to the result of 4. 1, this value appears when the simulation model runs at 9.176μs. The rise-time (RT) is 3.174μs (from 6.002μs to 9.176μs) and the full-width-half-maximum (FWHM) is 1.684μs (from 8.314μs to 9.998μs). The RT and FWMH increased by 3.591μs and 1.37μs respectively, compared with the result of swPCD.

Fig 4.4 presents the result of detecting a plane wave by fswPCD in time domain,when the radius of top surface of cylinder r = 9.54mm, the longitudinal length of

fswPCD H = 19.08mm.

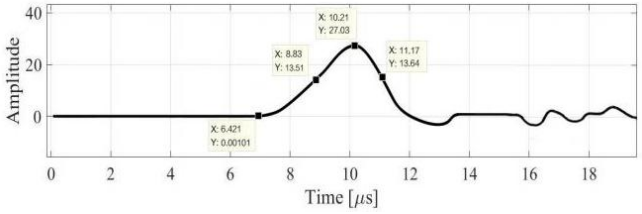

Fig 4.4 the result of detecting a plane wave by fswPCD in time domain , r=9.54mm, H=19.08mm

Under this condition, the peak-normalised output is 27.03mV, reduced by 28.5% (10.75mV) compared to the result of 4. 1, this value appears when the simulation model runs at 10.21μs. The rise-time (RT) is 3.789μs (from 6.421μs to 10.21μs) and the full-width-half-maximum (FWHM) is 2.34μs (from 8.83μs to 11.17μs). The RT and FWMH increased by 3.475μs and 2.026μs respectively, compared with the result of swPCD.

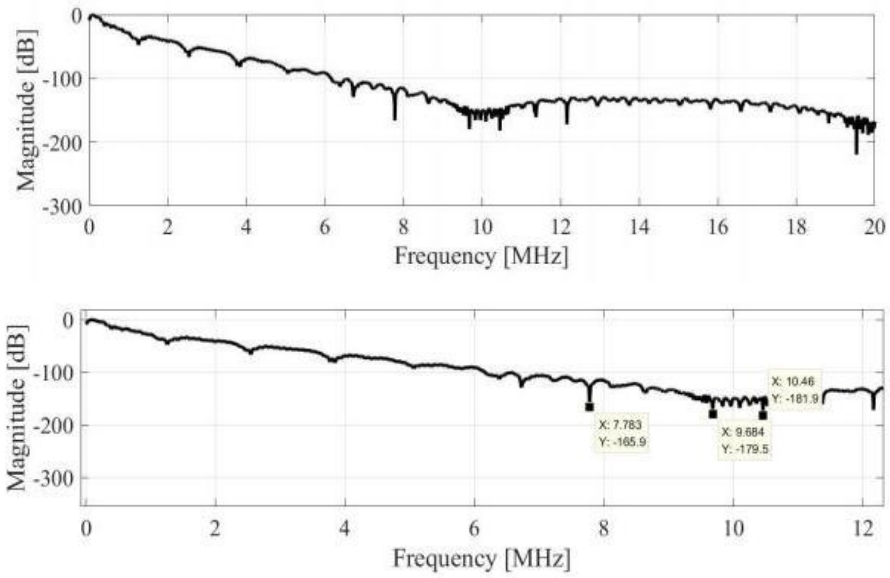

Fig 4.5 the result of detecting a plane wave by fswPCD in frequency domain,r=9.54mm, H=19.08mm . (a) the whole spectra with 10 stages (b) the spectra with frequency＜12MHz.

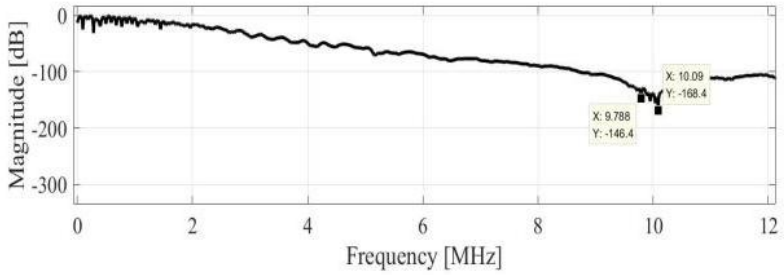

Fig 4.6 the spectra of swPCD with frequency＜12MHz

Since the experimental results have no significant difference in the frequency domain under the conditions of three different detecting surfaces for the fswPCD, the frequency domain result of one case with the largest curvature (that is r=9.54mm, H=19.08mm) is selected for comparison. Fig 4.5(b) indicates that in the interval of 0-12Mhz, the magnitude value decreases from 0dB to around -180dB, and the lowest value is - 181.9dB. Fig 4.6 presents the frequency spectra with frequency ＜ 12MHz, the magnitude value decreases from 0dB to around -150dB, and the lowest value is -168.4dB. In the same frequency range, the magnitude value of fswPCD is about 20~30dB lower than that of swPCD.

References

[1] Suslick, K. S. (1990). Sonochemistry. Science, 247(4949), 1439-1445.

[2] Mason TJ. (1996). Advances in sonochemistry (Vol. 4). Elsevier.

[3] Young, FR.(1999). Cavitation. World Scientific.

[4] Suslick K.S.(1988). Ultrasound: Its Chemical, Physical and Biological Effects,

VCH Publishers, New York.

[5] Price G. (1992). Current Trends in Sonochemistry, RSC, Cambridge.

[6] Kis-Csitári, J., Kónya, Z., & Kiricsi, I. (2008). Sonochemical synthesis of inorganic nanoparticles. In Functionalized Nanoscale Materials, Devices and Systems (pp. 369-372). Springer, Dordrecht.

[7] Muthukumaran, S., Kentish, S. E., Stevens, G. W., & Ashokkumar, M. (2006).

Application of ultrasound in membrane separation processes: a review. Reviews in chemical engineering, 22(3), pp.155-194.

[8] Cavalieri, F., Zhou, M., & Ashokkumar, M. (2010). The design of multifunctional

microbubbles for ultrasound image-guided cancer therapy. Current topics in medicinal chemistry, 10(12),1198-1210.

[9] Bhaskaracharya, R. K., Kentish, S., & Ashokkumar, M.(2009).Selected

applications of ultrasonics in food processing. Food Engineering Reviews, 1(1), 31.

[10] Ashokkumar, M.(2011).The characterization of acoustic cavitation bubbles–an overview. Ultrasonics sonochemistry, 18(4), 864-872.

[11] Leighton T. (1997). The acoustic bubble. Academic Press, ISBN.

[12] Coussios CC. and Roy RA. (2008). Applications of acoustics and cavitation to noninvasive therapy and drug delivery. Annual Review of Fluid Mechanics, 40, pp.395-420.